

Influence of additional inlet flow on the prerotation and performance of centrifugal impellers

Influence d'un écoulement d'admission additionnel sur la pré-rotation et la performance des roues à aubes centrifuges

ANDREJ PREDIN, *Ass. Prof. Dr., univ. dipl. ing., Head of the Laboratory for turbine machines, University of Maribor, Faculty of Mechanical Engineering, Smetanova 17, SI-2000 Maribor, Slovenia. E-mail: andrej.predin@uni-mb.si*

IGNACIJO BILUŠ, *MSc., univ. dipl. ing., Researcher, University of Maribor, Faculty of Mechanical Engineering, Smetanova 17, SI-2000 Maribor, Slovenia. E-mail: ignacijo.bilus@uni-mb.si*

ABSTRACT

In this paper we present the results of our experimental analysis regarding the influence of additional flow when added at the radial impeller entrance eye. This analysis was done on both operating and prerotation flow characteristics. The experimental system tested was arranged to operate using air. The additional flow adding system (AFAS) was placed at the entrance eye of the impeller through the guide system, which consists of the spiral volute at the entrance, ring guide pipe (where the guide vanes are placed), and a ring – like hollow at the end of the AFAS. The ring – like hollow was placed near the shroud at the entrance edge of the impeller blades. The guide vanes in the AFAS were placed in the axial direction, so that the added flow had no swirl component. The operating regime was tested, whereby the AFAS was filled by the flow under atmospheric pressure (non-forced loading). A good influence was evident on the operating characteristic. The stable operating range was enlarged and the operating noise decreased. The achieved impeller head and the overall efficiency increased.

RÉSUMÉ

Cet article présente les résultats de notre analyse expérimentale concernant l'influence d'un écoulement additionnel introduit à l'œil d'entrée radiale d'une roue à aubes. Cette analyse a été faite pour les caractéristiques de l'écoulement en fonctionnement et également en pré-rotation. Le dispositif expérimental a été adapté pour fonctionner en air. Le système d'apport de l'écoulement additionnel (AFAS) a été placé à l'œil d'entrée de la roue à aubes à travers le système guide, qui comprend la volute d'entrée en spirale, le tuyau guide en anneau (là où sont placées les ailettes de guidage), et une cavité en forme d'anneau au bout de l'AFAS. Cette cavité en anneau a été placée près de l'anneau d'étanchéité au bord d'entrée des aubes. Les ailettes de guidage dans l'AFAS ont été placées dans la direction axiale pour que l'écoulement supplémentaire n'ait pas de composante tourbillonnaire. Le régime de fonctionnement a été testé, l'AFAS étant le siège de l'écoulement induit par la pression atmosphérique (sans mise en charge supplémentaire). On a pu observer une nette amélioration des caractéristiques. La plage de fonctionnement stable a été agrandie et le bruit a diminué. La charge de la turbine obtenue et l'efficacité globale sont améliorées.

Keywords: Radial turbomachines; operating characteristics; additional entrance flow; operating noise.

1 Introduction

Most radial impellers with the specific speed n_q between 20 and 35 rpm have an unstable operating characteristic (flow rate – head curve ($Q-H$)). The stable part is in the area of larger operating flow rates and is relatively narrow in respect of the whole achieved flow rate area, up to around 40 percent of the interval between minimal and maximal achieved flow rate. This fact limits the fan/pump employability in the sense of its wider regulated operating possibilities at the current flow rate or head, while the pump operating at small flow rate (in the unstable operating range) is unstable. It is acknowledged that, during small operating flow rates, a secondary flow, Neumann [1], is created at the impeller entrance

(Figure 1a). This flow creates the 'back flow – BF' which affects the upstream into the intake pipe (Figure 1a) at small operating flow rates and creates the prerotation flow in the intake pipe at some distance before the impeller entrance, in fact, a distance up to three pipe diameters. This circulating secondary flow also chokes the main flow at the impeller entrance and, therefore, the active impeller trailing blade edge is narrowed. When the operating flow rate increases up to a flow rate somewhere between critical flow rate $Q_{cr} = 0.35 \text{ m}^3/\text{s}$ (where the $Q-H$ characteristic passes the unstable into a stable operating range), and optimal flow rate $Q_{BEP} = 0.825 \text{ m}^3/\text{s}$ for rotational speed $n = 1800 \text{ rpm}$ (where the fan/pump is the most efficient, at BEP) the secondary flow theoretically disappears (Figure 1b).

Revision received March 20, 2002. Open for discussion till August 31, 2003.

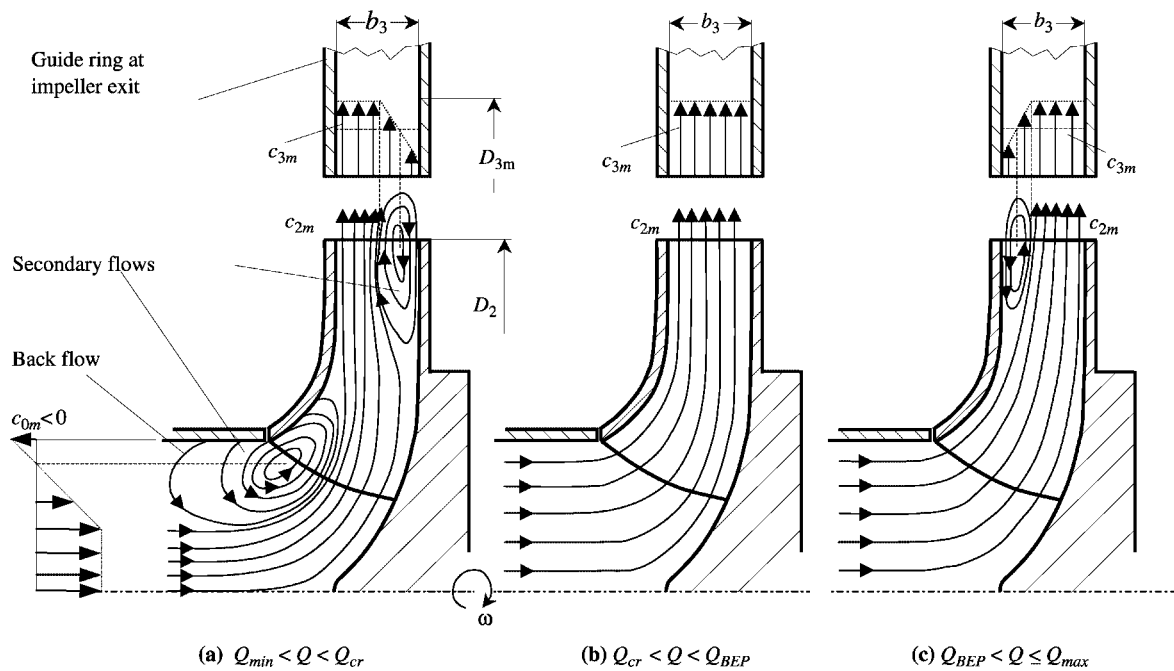


Figure 1 Secondary flow at different places by different operating flow rates.

With a further increase in the operating flow rate or flow rate through the fan/pump the secondary flow theoretically appears only at the impeller blade exit edge (Figure 1c) near the tip shroud of the impeller. All these situations created at different places produce secondary flow, which has an affect on the meridional velocity at the impeller exit as shown in Figure 1. To confirm this statement measurements were taken of the flow velocity at the impeller exit diameter $D_{3m} = 0.614$ m. The prerotation flow strength and the sense of rotation in the intake pipe of the examined fan or pump model, were also measured at a distance of three pipe diameters before the impeller entrance eye.

Sipos [2] examined the secondary flows of radial compressors. He concluded that the phenomenon of secondary flows is very complex, but his experimental results confirmed the situation described in Figure 1. Mizuki and Oosawa [3] examined the unsteady flow patterns throughout the centrifugal compressor system during the rotating stall and the surge. The performed results also confirmed the existence of the back flow at the impeller entrance during part-load operating.

The basic idea for eliminating the affects of secondary flows during fan/pump operating by small operating flow rates was to perform the Eck's theory (Eck [4]) of additional flow added at the impeller entrance. We tried, therefore, to decrease the prerotation flow in the intake pipe, improve the overall efficiency, Predin [5,6], especially in the area of small operating flow rate and increase the stable operating range of the tested pump model.

2 Experimental impeller with a system for adding additional flow and inserting an anemometer with straight blades into the intake pipe

A radial impeller with 11 back-bent untwisted blades (Figure 2, pos. 1), with diameters $D_1 = 0.36$ m, $D_2 = 0.6$ and, intake

$\beta_1 = 23^\circ$ and exit blade angle $\beta_2 = 25^\circ$, constant width $b_1 = b_2 = 0.05$ m is used for testing. At the impeller exit the diffuser with parallel walls with 24 pivoted guide vanes (Figure 2, pos. 2) and 12 stay vanes (Figure 2, pos. 3) is placed. The AFAS system consists of a spiral guide volute (Figure 2, pos. 4), ring guide pipe with inner pipe (Figure 2, pos. 5) and outside pipe (Figure 2, pos. 6), where the guide vanes (Figure 2, pos. 7) are placed. At the end of the ring guide pipe is a ring – like hollow with a cleft between the walls of $r = 0.005$ m. The ring – like hollow distance can be changed throughout a range of between 0.003 up to 0.006 m. The anemometer impeller (Figure 2, pos. 8) with 6 straight blades directed in an axial direction is placed into the intake pipe. Two inductive probes (TURCK Bi-M12-AP6X) are placed on the outside pipe wall (Figure 2, pos. 9). This anemometer measures the prerotation flow in the intake pipe. The flow rate through the AFAS is up to 10% of the maximal flow rate at BEP and is given in relative form by λ in diagram (Figure 5). The suitable exit flow velocity from the AFAS into the impeller eye is 2.5 times larger than the main flow entrance velocity c_v , Eck, [4]. The basic Q - H characteristic is unstable (Figure 3). The stable part is within an operating range between $Q/Q_{BEP} = 0.75$ up to $Q/Q_{BEP} = 1.25$ at 1800 rpm.

3 Impeller operating characteristics, exit flow velocities and prerotation flow

Maximal impeller pump head coefficient $\psi = 0.937$ is achieved at critical flow rate Q_{cr} ($Q/Q_{BEP} = 0.75$), where prerotation flow in the entrance pipe changes its sense of rotation (Figure 3). Below this flow rate the prerotation flow has a direction equal to the impeller's sense of rotation, and above the critical flow rate has a direction opposite to the impeller's sense of rotation. It is interesting that the prerotation flow changes its direction

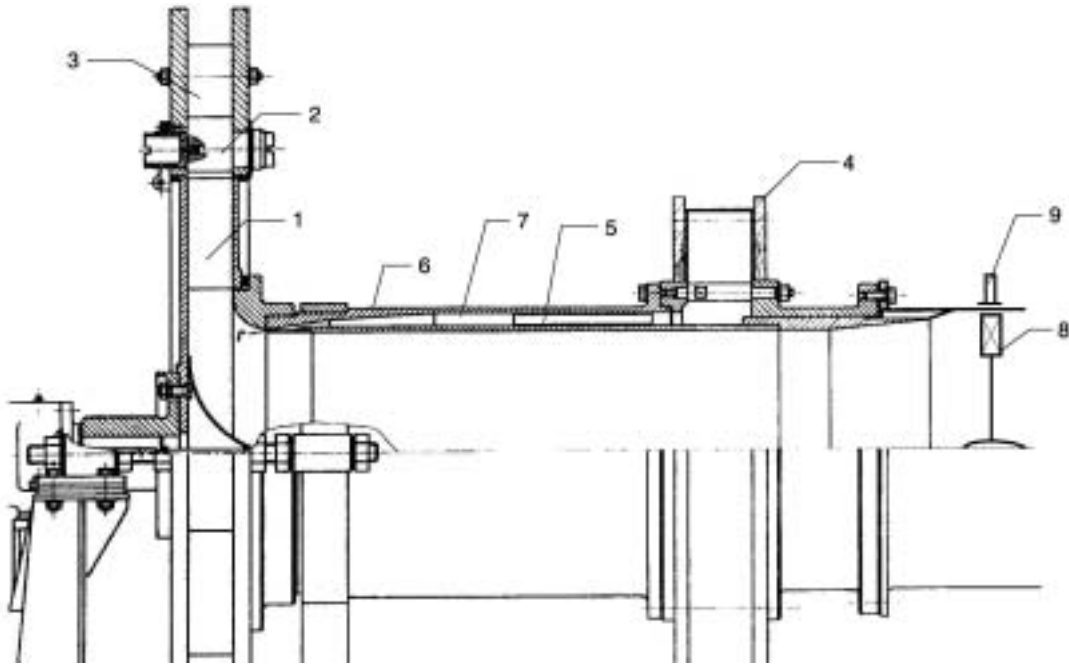


Figure 2 Testing model system with AFAS.

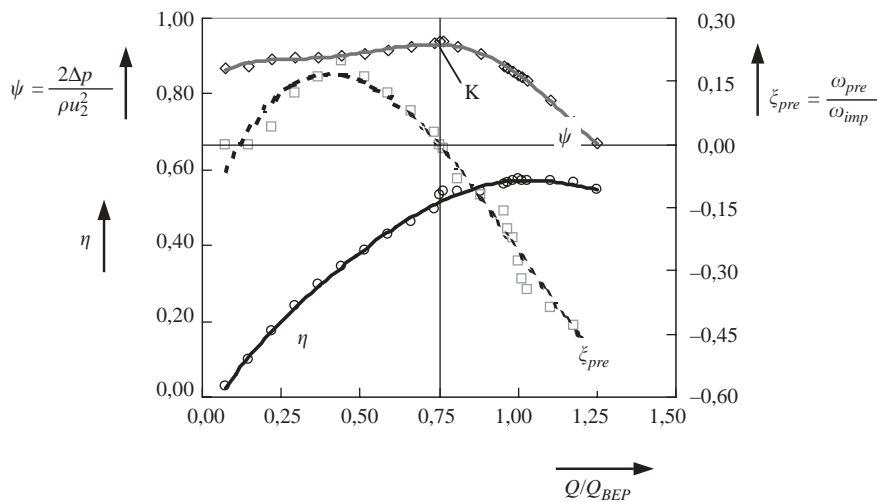


Figure 3 Head curve, efficiency curve and prerotation curve, without added flow.

sooner than the impeller design flow rate as it follows from the Euler's entrance velocity triangles (Figure 4). This shows that the prerotation flow is arranged in the direction of lowest resistance. In this direction the flow path is as short as possible. In this way the friction losses at the impeller eye entrance decrease. At the design operating point the optimal operating absolute flow velocities in circumference diameter should be achieved. As we already know, the energy difference achieved at flow rates in the area of lower, under optimal flow rates, increases, whilst at larger, over-optimal flow rates, the energy difference decreases. However, when following the impeller operation out of the design operating point, it cannot be predicted whether the absolute flow velocity in the circumferential direction will be zero ($c_{1u} = 0$) as it is simply shown by the Euler's entrance flow velocity triangles (Figure 4b).

The flow velocity component in the tangential direction at the entrance diameter D_1 appears in the direction of the impeller

rotation (same direction as u_1) when operating at under-optimal flow rates. The cause of this flow component creation can probably be found in the appearing secondary flow near the entrance edge of the impeller blades and in the gap between the tip impeller shroud and the fan/pump casing. This part of the flow penetrates through the gap between the shroud at the entrance edge and pump casing back to the impeller eye where the flow rotates by velocity u_1 near the tip impeller shroud because of the higher pressure at the impeller exit. This is the tongue of flow that over the flow viscosity creates the prerotation flow in the intake pipe up to three-intake diameter length ($l \approx 3D_v$) from the impeller eye. According to this operating regime it could be considered that the circulation around the blades increases because of the larger blade load (achieving larger energy difference), which causes the increase of pressure at the impeller exit. The strengthening of circulation around the impeller blades can be explained by the entrance flow angle decrease α_1 (Figure 4a) at the entrance of the

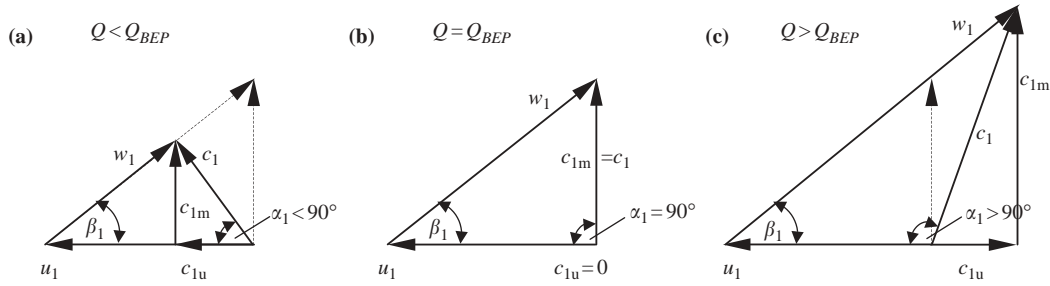


Figure 4 Euler's entrance velocity triangles at different operating flow rate.

impeller channels or by the flow intake on the blade, where the flow cutting and flow separation from the blade suction surface appears. While the flow vortices and flow separation cause pressure decrease, the part of the flow from the area of higher pressure (near exit edge of the impeller blade) penetrates to the area of lower flow pressure and in this way strengthens the circulation around the blades.

By increasing the flow rate above the optimal flow rate, the absolute flow velocity in the circumferential direction at the entrance diameter creates a prerotation flow in the opposite direction to the impeller rotation. To achieve any increased operating flow rates the prerotation flow must be diverted before it reaches the impeller eye in the direction of the smallest resistance, that is, in the opposite direction to the impeller rotation (Figure 4c). An increase in the flow entrance angle and, thus, a shorter entrance path are achieved using this flow redirection. The main reason for this increased circulation in the impeller channels is probably the increased circulation flow in the individual impeller channels. In this operating regime (over-optimal flow rates) the entrance flow angle α_1 increases over 90° . The result of bigger entrance angle would be flow separation appearing near the pressure blade surface at the entrance blade edge. Circulation flow around the impeller blade is created in the opposite direction to the existing circulation around the impeller blade because of this flow separation (similar to operating with under-optimal flow rates). In this way the circulation around the blade decreases. The result

of this decreased circulation around the blade is decreased circulation at the exit diameter D_2 and, consequently, the energy difference achieved by the impeller. The operating characteristic of radial impellers is mostly unstable with the stable part of it in the area of larger operating flow rates (larger than the critical flow rate), where the operating characteristic has a decreasing tendency. According to this, the achieved energy difference of the impeller in the stable part of the operating characteristic decreases with the increasing flow rate.

When operating with additional flow the $Q-H$ characteristic curve becomes more stable, in effect from the flow rate ratio $Q/Q_{BEP} = 0.6$ up to 1.25. The achieved head coefficient ψ and impeller operating efficiency η are also increased at almost all operating flow rates (Figure 5). It is interesting that at small operating flow rate the majority (75%) of the common operating flow rate (flow rate from the main intake pipe plus flow rate from AFAS) is taken from the AFAS (Figure 5, curve - λ).

The exit flow velocities from the impeller at the measuring diameter D_{3m} , between the impeller blade trailing edge and intake edge of the guide-vanes in the guide apparatus, were measured to confirm the existence and influence of appearing secondary flows in the impeller. The anemometer system DISA 55 M01 was used with one channel probe DISA 55 P11. The probe was placed into the flow at the apparent streamlines in the impeller or guide apparatus width direction. From the measured results (Figure 6), whilst operating without additional flow added at the

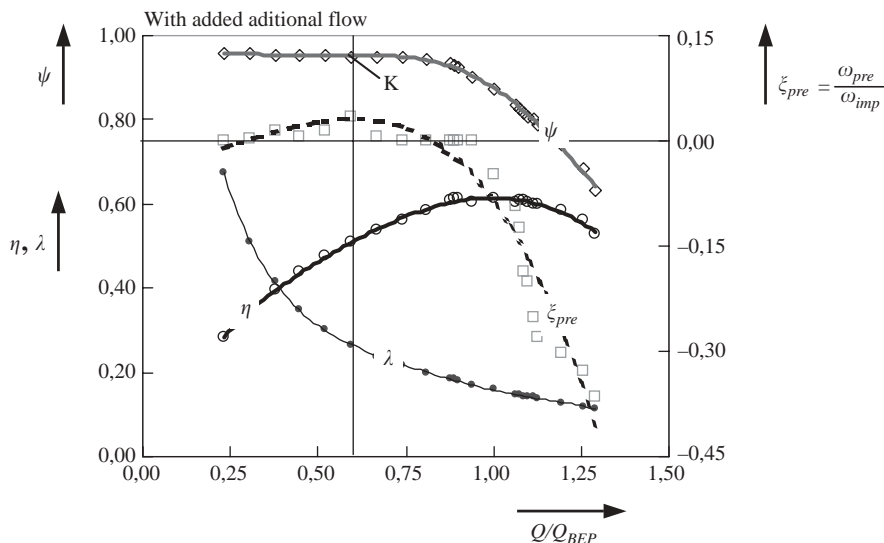


Figure 5 Head curve, efficiency curve and prerotation curve, with added flow.

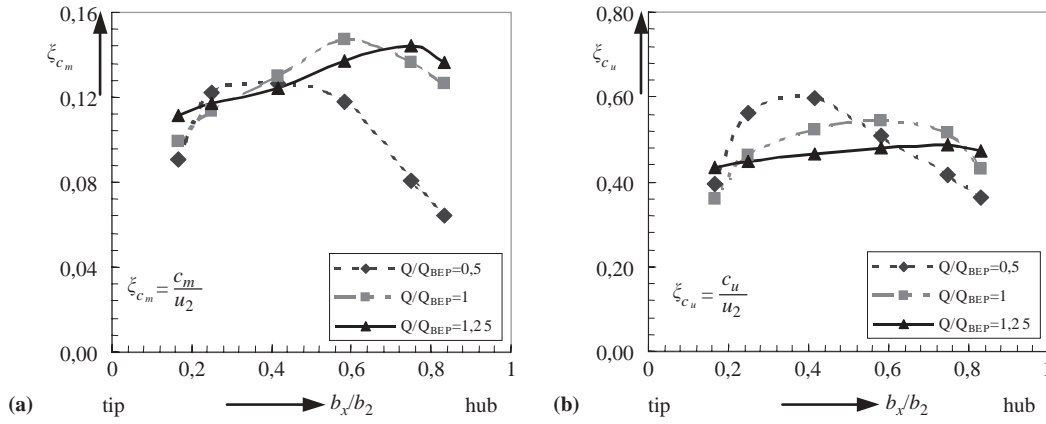


Figure 6 Exit flow velocities from the impeller; (a) meridional and (b) tangential dir.

impeller entrance, similar velocity distribution in width direction was confirmed as predicted (Figure 1), after considering the created secondary flows in the impeller during operating at different operating flow rates.

When operating with flow rates smaller than the optimal flow rate the velocity increase near the shroud at the impeller blade exit edge is evident from both absolute velocities in meridional (Figure 6a) and in the tangential direction (Figure 6b). With a flow rate increase up to the optimal flow rate the velocities are more equal over the width than when operating with smaller flow rates. The flow velocities near the impeller hub shroud increase with further flow rate increase. An equal or similar situation is evident in both absolute flow velocity directions and accordingly the existence and position of the secondary flows is confirmed. Exit velocities are also changed by the additional flow added at the impeller entrance (Predin [6], and Predin and Popović [7]) in the width direction. The velocity increase, during operating with added flow, is evident from the measured data (Figure 7). The increased velocities are evident at the tip shroud as well as at the total impeller width (Figure 7a) and accordingly to this an improved impeller load in the width direction can be concluded. This could be the reason for the increased efficiency and energy difference or increased head coefficient ψ . The differences between the velocity profiles at different operating regimes decrease when the impeller operates with the flow rate larger than the optimal flow rate ($Q/Q_{BEP} = 1$). By operating with maximal over-optimal flow rates ($Q/Q_{BEP} = 1.25$), the

differences are minimal (up to 11%). Good agreement between the measured velocity curves at both operating regimes is evident (Figure 7c). The velocities are practically equal at the larger part of the impeller width.

Generally, it can be concluded that the additional flow added at the impeller intake, near the tip (front) shroud, has a positive influence on the impeller-operating load. A larger operating load is achieved with better exploitation of the impeller width. At the same time the absolute flow velocity at the impeller exit (in the tangential direction) increases the pressure difference and the energy difference. The additional flow has a beneficial effect on larger energy differences, especially at the area of under-optimal flow rates.

3.1 Prerotation flow

Most fluids crossing the turbo machines are viscous fluids. The real flow through the turbomachine is turbulent in major cases. Therefore the flow in the entrance pipe, as well as in impeller channels, must be treated as a turbulent viscous flow. Indeed, the bases of the prerotation flow, which is the result of the boundary layer separation in the intake pipe, are: (1) the relative flow whirls at the individual impeller channels, (2) the circulation flows around the impeller blades and from these flows circulation flow formed at the entrance and exit diameters of the impeller.

Circulation flow, or circulation in general, can be represented by the curve integral of the general vector quantity, for example

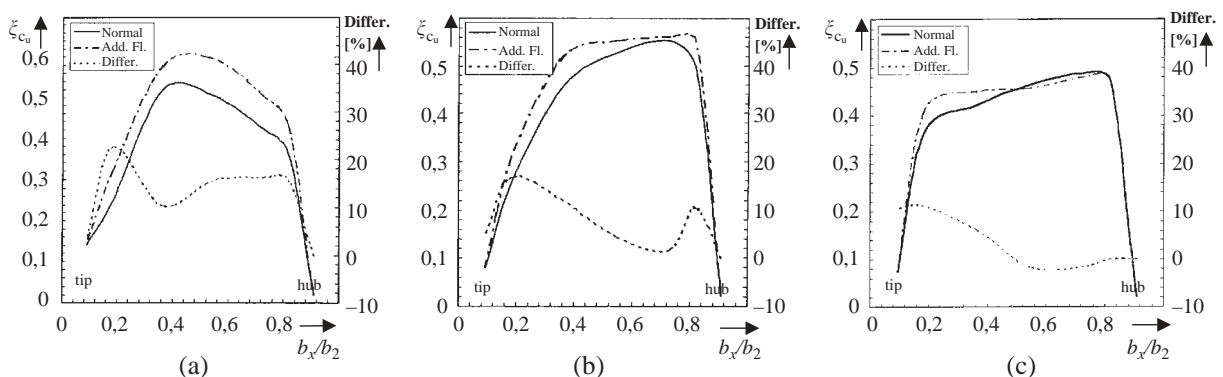


Figure 7 Velocity profiles in impeller width direction, (a) at $Q/Q_{BEP} = 0.5$, (b) $Q/Q_{BEP} = 1.00$, (c) $Q/Q_{BEP} = 1.25$.

flow velocity

$$\Gamma = \oint_L \vec{v} \cdot d\vec{l}, \quad (1)$$

where \vec{v} is the flow velocity vector multiplied scalarly along the curve L . While the velocity vector is $\vec{v} = (v_x, v_y, v_z)$ and $d\vec{l} = (dx, dy, dz)$, the Eq. (1) can be written in the following form

$$\Gamma = \oint_L (v_x dx + v_y dy + v_z dz). \quad (2)$$

Considering the relationship between $\vec{v} \cdot d\vec{l} = v \cos \alpha dl = v_t dl$ we get

$$\Gamma = \oint_L v_t dl \quad (3)$$

where v_t is tangential velocity that flows around the rigid body formed by curve L . In this case Eq. (3) can be used for determining of the circulations. The circulation at the entrance diameter D_1 can be written as

$$\Gamma_1 = c_{1u} \pi D_1 \quad (4)$$

and analogy at the diameter D_2

$$\Gamma_2 = c_{2u} \pi D_2 \quad (5)$$

where c_{1u} and c_{2u} are the absolute flow velocities in the circumferential (tangential) direction at the entrance and exit impeller diameter, respectively. The circulation in the individual impeller channel in one plain, for example in the plain of the middle stream surface of the impeller channel, can be determined by tangential velocity integrating along the walls of the impeller channel at the particular channel parts (Figure 8).

$$\begin{aligned} \Gamma_K = & - \int_A^B c_{1u} dAB + \int_C^B w_t dBC + \int_D^C c_{2u} dCD \\ & - \int_D^A w_s dDA \end{aligned} \quad (6)$$

or

$$\Gamma_K = -c_{1u} \frac{D_1}{z_r} + w_t l_{lop} + c_{2u} \frac{D_2}{z_r} - w_s l_{lop} \quad (7)$$

$$\Gamma_K = -c_{1u} t_1 + w_t l_{lop} + c_{2u} t_2 - w_s l_{lop} \quad (8)$$

where t_1 is pitch at the entrance and t_2 at the exit diameter, l_{lop} is blade curved length, w_t is the relative flow velocity at the pressure side of the blade and w_s at the suction side, respectively. In the Eq. (8) the theoretical determination of the relative flow velocities

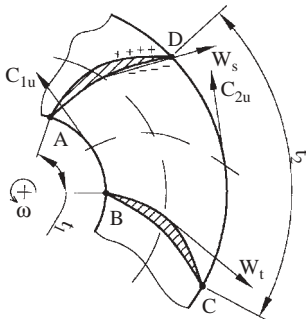


Figure 8 The circulation in the individual impeller channel.

w_s and w_t , which change in the direction of the impeller blade, is problematic. Eckert and Schnell [8], defined the difference in the relative flow velocities between the pressure and suction face of the blade as follows

$$(w_s - w_t) = 4(c_{2u} - c_{3u}), \quad (9)$$

and

$$c_{2u} - c_{3u} = \frac{\pi D_2^2 b_2 c_{3u}}{8 z_r S} \sin \beta_2 \quad (10)$$

where b_2 is the impeller width on the impeller exit diameter, z_r number of impeller blades, β_2 blade angle and S moment of cross sectional area element bdr of impeller blade in the elevation about the axis with the lever r , according to Pfleiderer [11]

$$S = \int_{r_1}^{r_2} br dr \quad (11)$$

Using these relationships in Eq. (8) we get the following equation for circulation in the impeller channel:

$$\Gamma_K = -c_{1u} t_1 + c_{2u} t_2 - l_{lop} \frac{\pi D_2^2 b_2 c_{3u}}{2 z_r S} \sin \beta_2, \quad (12)$$

which can be calculated on the bases of the impeller pump geometry.

The circulation around the impeller blade can be calculated according to the energy difference achieved by the pump. The torque or the moment that it is achieved is

$$M = z_r \int_{r_1}^{r_2} \Delta p br dr \quad (13)$$

where Δp is the pressure difference which is achieved by the impeller. Assuming this pressure difference is equal to the one due to the energy theorem for relative flow we get with ρ as fluid density (considering that the pressure difference is equal to the difference of the squared relative flow velocities between the impeller entrance and exit, multiplied by the fluid density);

$$\Delta p = \frac{\rho}{2} (w_1^2 - w_2^2) \quad (14)$$

and by introducing the impeller angular speed w and mass flow rate through the impeller \dot{m} the specific energy;

$$Y_{th} = g H_{th} = \frac{w z_r \rho}{2 \dot{m}} \int_{r_1}^{r_2} (w_1^2 - w_2^2) br dr, \quad (15)$$

which can be equated to the Y_{th} term according to Euler's principal turbine equation. Inserting after Sigloch [9], Γ_L as the circulation around the impeller blades, Eq. (15) is converted into:

$$Y_{th} = g H_{th} = w \frac{z_r \Gamma_L}{2 \pi} = w (r_2 c_{2u} - r_1 c_{1u}) \quad (16)$$

from where the circulation around the individual impeller blade can be presented as

$$\Gamma_L = \frac{2 \pi}{z_r} (r_2 c_{2u} - r_1 c_{1u}) = \frac{\pi}{z_r} (D_2 c_{2u} - D_1 c_{1u}). \quad (17)$$

According to the circulations, determined at the impeller entrance diameter Γ_1 Eq. (4), at exit diameter Γ_2 Eq. (5), in impeller channel Γ_K Eq. (12) and around the impeller blade Γ_L Eq. (17), two equilibrium equations, based on two different circulation

directions (circulation in impeller channel and circulation around the impeller blade), can be written as

$$\Gamma_2 = \Gamma_1 + z_r \Gamma_K, \quad (18)$$

$$\Gamma_2 = \Gamma_1 + z_r \Gamma_L \quad (19)$$

The Eq. (18) can be written for example, for the central part of impeller channels, and Eq. (19) for the central part of the blade from the entrance up to the exit blade edge. Equation (19) represents the flow properties following the blade wake. In the case of an 'ideal' potential flow and a vanishing thin blade without any stall the circulations, around the blades and in the impeller channels are equal to one:

$$\Gamma_L = \Gamma_K. \quad (20)$$

From both equilibrium Eqs. (18), (19) it is also evident that the circulating flow around the blades influences the circulation at the exit diameter Γ_2 and, therefore, also affects the energy difference of the impeller (achieved fan's head). The same can be concluded for the circulation in the impeller channels. According to this, it is possible to conclude that the fan/pump operating characteristic shape depends on the ratio of the circulation around the impeller blades and circulation in the impeller channels. The causes of the appeared circulating flows are different but they are connected. Coriolis and body force due to the curved blades drive the circulating flow in the impeller channel. The circulating flow around the impeller blade is created as a result of pressure difference between pressure and suction face of the blade surface (flow separation). The cause of this pressure difference is different relative flow velocities near the blade surface, which are the cause of appeared circulation around the blade.

Equality of both circulations, therefore, exists in the following relationship

$$\pi(D_2 c_{2u} - D_1 c_{1u}) = \left(\frac{\pi D_2}{z_r} c_{2u} - \frac{\pi D_1}{z_r} c_{1u} + l_{lop}(w_t - w_s) \right) \quad (21)$$

By rearranging Eq. (21) we get the following relationship for absolute flow velocity in circumferential direction at the inlet diameter D_1 :

$$c_{1u} = \left(\frac{D_2}{D_1} \right) c_{2u} + \frac{z_r l_{lop}}{\pi D_1 (z_r - 1)} (w_t - w_s) \quad (22)$$

from where we can find absolute flow velocity in the circumferential direction at the outlet diameter D_2 at which the equivalent velocity c_{1u} equals zero. This theoretically also means that the prerotation flow in the inlet pipe does not exist. Under these conditions absolute flow velocity in the circumferential direction at outlet diameter D_2 is

$$c_{2u} = \frac{l_{lop} z_r}{\pi D_2 (z_r - 1)} (w_s - w_t) \quad (23)$$

Considering Eqs. (9) and (10) the following formula can be derived:

$$c_{2u} = \frac{l_{lop} D_2 b_2 \sin \beta_2}{2(z_r - 1)S} c_{3u} \quad (24)$$

The formula shows that the absolute flow velocity in the circumferential direction at the outlet diameter depends on geometry

(l_{lop} , D_2 , b_2 , β_2 , S) and absolute velocity c_{3u} behind the exit diameter, which considers the flow slip and impeller imperfection respectively. All parameters mentioned above can be combined in a constant K_R and written as:

$$c_{2u} = K_R c_{3u} \quad (25)$$

From Eq. (25) it is evident, that K_R considers the slip of the flow at the impeller exit. Based on this formula the correct derivation of equations can be assumed, because the result is logically connected with Eck's [4] results.

This increased circulating flow causes the secondary flows near the entrance blade edge in the intake pipe, and, similarly, as in the case of 'created flow – tongue' drive the prerotation flow some distance before the impeller eye in the intake pipe over the flow viscosity in the opposite direction of the impeller rotation. The directional change applies gradually which is evident from the measured results, while after operating flow rate change, the prerotation flow appears after a short time period, when new operating conditions (angular speed of the anemometer impeller) are stabilized.

The most effective operating point (BEP) is, in most cases, somewhere in the middle of the stable operating part. If we start our observations from Eq. (19) we can see that the circulation at the exit diameter of the fan/pump impeller is equal to the circulation sum of all circulations around the blades plus the circulation at the intake diameter. For the area of the under- and/or over-optimal flow rates, two conclusions (Figure 9) can be made:

- (1) Constant circulation at the entrance diameter ($\Gamma_1 = const.$) when the circulation around the blades must be changeable so, that it is bigger than the circulation at optimal operating flow rate in the area of flow rates smaller than the optimal flow rate, and smaller when the operating flow rates are larger than the optimal, as follows from the operating curve (flow rate-head curve).
- (2) The constant circulation around the blade ($\Gamma_L = const.$) when the circulation at the entrance diameter must be changeable, so, that it is larger in the area of under-optimal flow rates and, in the area of over-optimal flow rates, smaller than the circulation by optimal operating at the BEP.

In reality both cases interact together, so it is difficult to say which one is constant for different operating flow rates. The fact is that the prerotation flow is created in the opposite direction to the impeller's sense of rotation in the area of over – optimal flow rates as follows from the second prediction. Creation of the prerotation flow is, therefore, the result of the integrated circulations around the impeller blades, as well as the result of the integrated circulations in the impeller channels and circulation at the entrance diameter of the impeller. All these acting parameters depend on the impeller geometry, on operating conditions, and on operating flow rate.

4 Comparison of the head/efficiency – flow rate curves

When comparing the characteristics, curves ($Q/Q_{BEP} - \psi$), when operating with and without added flow (Figure 10a), it is

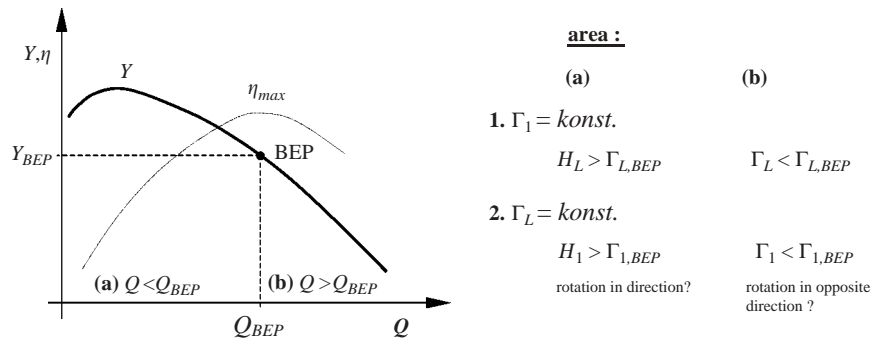


Figure 9 Typically operating characteristic of the radial impellers.

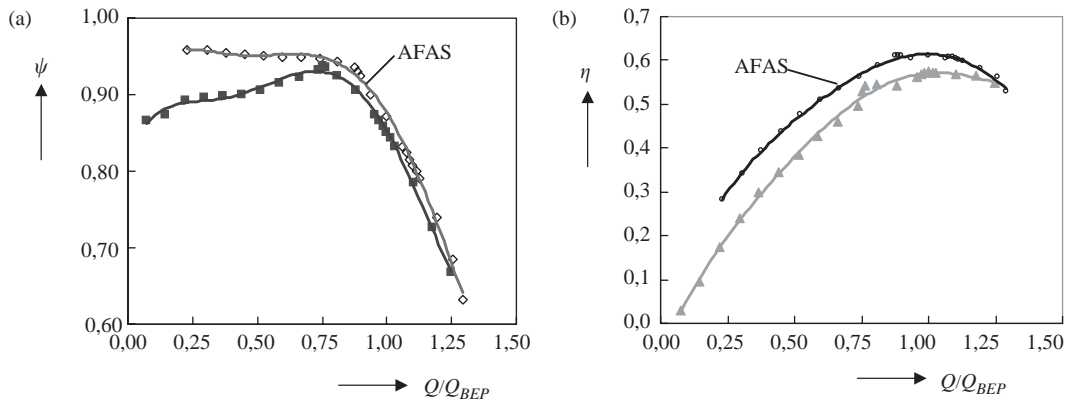


Figure 10 Flow – rate head (a), and Flow – rate efficiency (b) comparison, with and without additionally added flow at the impeller entrance eye.

evident that the head number ψ has been increased from the critical point K in the stable area as well as in the unstable area. The average value of the head number ψ , at the stable part of operating characteristic curve ($Q/Q_{opt} - \psi$) when operating with additionally flow, has been increased up to 7.6% relative to the head coefficient by operating without added flow. In this case (K_{AFAS} to K) a higher head coefficient increase up to 10% is achieved. In the whole area of operating flow rates, at impeller operating with additionally added flow, the head coefficient is increased. From this fact a suitable additional flow influence on the impeller operating characteristic can be concluded.

From the efficiency curves (Figure 10b), it is evident, that the efficiency increases with the additional flow, especially at the unstable operating part. The efficiency is increased up to 58.3% at minimal, and up to 1.2% at maximal flow rates with the additional flow. The higher efficiency increase is achieved in the area of smaller flow rates, but this increase is relative because of the small efficiency values. The real efficiency increase was achieved in the stable operating range, up to the critical flow rate, where the efficiency increases up to 12.5%. The overall efficiency at the optimal impeller-operating regime (at best efficiency point – BEP) by additional flow is increased by up to 8.2%.

When comparing the prerotation flow curves (Figure 11) it is evident, that with additional flow at the impeller entrance the prerotation flow changes its sense of rotation at larger operating flow rates than by operating without added flow. At small operating flow rates in the operating regime with added flow, the prerotation flow intensity is smaller or almost equal to zero prerotation. It is evident, that sense of rotation of prerotation flow is in accord with impeller’s sense of rotation only at the smallest operating flow

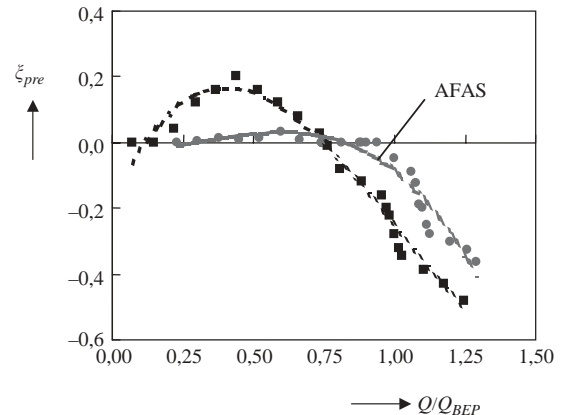


Figure 11 Prerotation flow intensity comparison.

rates (at operating regime with added flow). In contrast, when operating without added flow the prerotation flow with small flow rates has a direction that is equal to the impeller’s sense of rotation. With increased flow rate the prerotation flow in the opposite direction is as intensive during the operation without added flow as when operating with added flow. This shows that additional flow decreases the prerotation flow intensity.

5 Conclusions

According to the analyses of the prerotation flow in the entrance pipe it can be concluded that the prerotation flow appears as the result of the circulating flow activity in the impeller channels and/or around the impeller blades, which have (through the fluid friction) an influence on the whirl flow in the entrance pipe.

Prerotation flow changes its sense of rotation because of the prerotation direction change around the impeller blades, caused by different inlet angles of flow at the entrance rotor radii. Circulation around the impeller blades has, at small (under-optimal) flow rates, the same sense of rotation as circulation at the outlet radii. Therefore, it increases the energy difference and, because of the small inlet angles, causes separation of flow at the suction side of the blade inlet edge.

There are bigger inlet flow angles and separation at the pressure side of the blade edges by larger, over optimal flow rates, and prerotation around impeller blades, therefore changes sense of rotation into the opposite direction of circulation flow. This change of direction causes smaller energy difference and prerotation swirl to be achieved in the opposite direction to the rotor sense of rotation.

The strength of the prerotation flow depends directly on the circulation flow intensity around the impeller blades or in the impeller channels. The prerotation flow increases with the flow rate increase. This phenomenon can be predicted with suitable mathematical – numerical accession which will be the guide line for further investigations.

The additional flow added at the impeller entrance significantly improves the impeller load, Q - H characteristic and overall efficiency. At the same time the area of the stable part of the impeller operation is extended. The area of unstable operating Q - H characteristics is thereby decreased.

Adding additional flow at the impeller entrance can be recommended, because of its beneficial influence when wider control – in the sense of the frequent change of the operating flow rate – is needed. Using the variant of free suction (non-forced) of the additional flow is also recommended. The wider stable operating range provides better control than is possible without the additionally added flow.

The achieved energy difference (or pressure difference achieved by the impeller), as well as the overall efficiency increase with additionally flow, are recommended for all systems that operate over a long time period. The energy savings generated by the increased efficiency and achieved energy difference, are significant. For systems, which only operate occasionally, detailed calculations must be made between larger investment costs (for the variant, with the possibility of additionally added flow), and the achieved energy savings, in order to ensure normal lifetime of the system.

For the impellers with larger width (higher performance types for maximal flow rates, as well as maximal achieved pressure differences) using the conclusions given in this article, together with Eck's recommendations, it can be affirmed that this system for additional flow is almost a requirement.

Notations

b = impeller, guide ring width
 c = absolute flow velocity
 c_m = meridional absolute flow velocity
 c_u = circumferential or tangential absolute flow velocity
 c_v = main flow entrance velocity

D = diameter
 D_v = intake pipe diameter
 g = gravity
 H = pump head
 H_{th} = theoretical pump head
 K_R = constant
 l = distance
 l_{op} = blade curved length
 \dot{m} = mass flow rate
 M = torque
 n_q = specific speed
 p = pressure
 r = distance between inner and outside wall of ring – like hollow; radii
 S = moment of surface element
 t = blade pitch at diameter
 Q = flow rate
 u = peripheral velocity of impeller
 v_t = tangential velocity component
 v_x = velocity component in x direction
 v_y = velocity component in y direction
 v_z = velocity component in z direction
 w = relative flow velocity
 w_s = relative flow velocity on the blade suction side
 w_t = relative flow velocity on the blade pressure side
 Y_{th} = theoretical energy difference
 z_r = number of the impeller blades

Greek letters

α = angle of the absolute flow velocity
 β = blade angle
 Δ = difference
 Γ = circulation
 Γ_K = circulation in the impeller channel
 Γ_L = circulation around the impeller blade
 η = efficiency
 λ = flow rate ratio of additional flow flow rate/common flow flow rate
 ρ = density
 ξ_{cu} = non-dimensional coefficient of absolute flow velocity in tangential direction
 ξ_{pre} = prerotation flow non-dimensional coefficient
 ψ = head coefficient
 ω = angular speed
 ω_{imp} = impeller angular speed
 ω_{pre} = prerotation flow angular speed

Subscripts

0 = before impeller entrance
1 = entrance edge of impeller blades
2 = discharge edge of impeller blades
3 = entrance to guide ring
min = minimal

cr = critical
 max = maximal
 imp = impeller
 pre = prerotation

Abbreviations

AFAS = additional flow – adding system
 BEP = best efficiency point
 BF = back flow

References

1. NEUMANN, B. (1991). “The Interaction between Geometry and Performance of a Centrifugal Pump”, Mechanical Engineering Publications Limits, London, pp. 173–234.
2. SIPOS, G. (1991). “Secondary Flow and Loss Distribution in a Radial Compressor With Untwisted Backswept Blades”, *J. Turbomachinery*, 113, 686–695.
3. MIZUKI, S. and OOSAWA, Y. (1992). “Unsteady Flow Within Centrifugal Compressor Channels Under Rotating Stall and Surge”, *J. Turbomachinery*, 114, 312–320.
4. ECK, B. (1997). Ventilatoren, 5. Auflage, Springer-Verlag, Berlin/Göttingen/Heidelberg, pp. 310–311.
5. PREDIN, A. (1999). “Improved Operating Characteristic of Radial Turbomachines by Adding secondary Flow at Impeller Entrance Diameter”, XXVII-IAHR Congress, Graz, 22–27 August, 1999, Sec. B10 p. 123.
6. PREDIN, A. (1999). “Influence of Secondary flow on the Operating Characteristics of a Radial Impeller with Normal Width”, *J. Mech. Engrg.*, 45(1), 25–34.
7. PREDIN, A. and POPOVIČ, M. (1993). “Contribution to the Experimental Analysis of Fluid Flow in the Guide Wheel of Reversible Pump-turbine in Pump Mode”, *33rd Heat Transfer and Fluid Mechanics Institute Proceedings*, Sacramento USA, pp. 41–55.
8. ECKER, B. and SCHNELL, E. (1961). “Axial- und Radial-Kompressoren”, Springer Verlag, Berlin Göttingen, Heidelberg, p. 345.
9. SIGLOCH, H. (1993). Strömungsmaschinen, Grundlagen und Anwendungen, Car Hanser Verlag München Wien, pp. 82–83.
10. PREDIN, A. (1997). “Torsional Vibrations at Guide-Blade Shaft of Pump-Turbine Model”, *Shock and Vibration*, 4(3), 153–162.
11. PFLEIDERER, C. and POTERMANN, H. (1986). Strömungsmaschinen, Springer Verlag, 5th edition, Berlin, pp. 46–47.